Journal of ELECTRONIC MATERIALS, Vol. 45, No. 8, 2016
DOI: 10.1007/s11664-016-4599-x

Effect of $(Ca_{0.8}Sr_{0.2})_{0.6}La_{0.267}TiO_3$ on Phase, Microstructure, and Microwave Dielectric Properties of $Mg_{0.95}Zn_{0.05}TiO_3$ Synthesized by Polymeric Precursor Method

ABDUL NAEEM,[1] ASAD ULLAH,[1,4] TAHIRA MAHMOOD,[1] YASEEN IQBAL,[2] ASAD MAHMOOD,[1] and MUHAMMAD HAMAYUN[3]

1.—National Centre of Excellence in Physical Chemistry, University of Peshawar, Peshawar 25120, Pakistan. 2.—Department of Physics, Material Research Centre, University of Peshawar, Peshawar 25120, Pakistan. 3.—Department of Chemistry, Institute of Natural Sciences, University of Gujrat, Gujrat, Pakistan. 4.—e-mail: asadncepc@upesh.edu.pk

A number of compounds in the $(1-x)Mg_{0.95}Zn_{0.05}TiO_3$-$x(Ca_{0.8}Sr_{0.2})_{0.6}La_{0.267}TiO_3$ (x = 0 to 0.25) composition series have been obtained via a polymeric precursor route to investigate the effect of increasing $(Ca_{0.8}Sr_{0.2})_{0.6}La_{0.267}TiO_3$ proportion on the phase, microstructure, and microwave dielectric properties of the sintered ceramics. Composite powders having nanometric particles were obtained by calcining the precursors at 700°C. Refinement results revealed that these samples comprised a mixture of $Mg_{0.95}Zn_{0.05}TiO_3$ and $(Ca_{0.8}Sr_{0.2})_{0.6}La_{0.267}TiO_3$ ceramics. A combination of optimum microwave dielectric properties, i.e., dielectric constant of 25.17, quality factor of 58,754 GHz, and temperature coefficient of resonant frequency of −5.8 ppm/°C, was achieved for the x = 0.2 composition sintered at 1200°C.

Key words: Microwave dielectrics, electroceramics, quality factor, polymeric

INTRODUCTION

Microwave dielectrics have played an important role in the rapid development of advanced communication systems, due to their wide range of applications in terrestrial and satellite communication technologies such as the global positioning system (GPS), software radio, and direct broadcast satellite television (DBS TV).[1–4] The development of high-frequency wireless communication technology and the consequent growth of the related industry over recent decades have substantially increased demand for microwave dielectric materials. For practical applications in microwave devices, a dielectric material must have a reasonably moderate dielectric constant ($\varepsilon_r > 20$) for size miniaturization, higher quality factor ($Q \times f > 20{,}000$) for target frequency selectivity, and near-zero temperature coefficient of resonant frequency (τ_f) for temperature stability of the system.[5,6]

(Received October 11, 2015; accepted April 28, 2016; published online May 18, 2016)

Magnesium titanate ($MgTiO_3$) with ($R3$) symmetry is a promising microwave dielectric material, having $\varepsilon_r = 17$, $Q \times f = 160{,}000$ GHz, and $\tau_f = -51$ ppm/°C.[7] Huang et al.[8] reported enhanced $Q \times f$ for $Mg_{0.95}Zn_{0.05}TiO_3$ ceramic via partial replacement of Mg^{2+} with Zn^{2+} in $MgTiO_3$, but a high negative τ_f value rendered it unsuitable for commercial applications. Fortunately, it is possible to adjust the high negative τ_f of $Mg_{0.95}Zn_{0.05}TiO_3$ via forming a composite with another material having high positive τ_f value.[9] One such candidate material to compensate high negative τ_f values is $CaTiO_3$ with orthorhombic ($Pbnm$) structure, exhibiting $\varepsilon_r = 170$, $Q \times f = 6000$ GHz, and $\tau_f = +800$ ppm/°C.[10] Partial substitution of La^{+3} for Ca^{+2} in $CaTiO_3$ has been reported to improve the low $Q \times f$ of $CaTiO_3$.[11] Similarly, ε_r can be enhanced by partial substitution of Sr^{+2} for Ca^{+2}.[12] The authors also reported that $(Ca_{0.8}Sr_{0.2})_{0.6}La_{0.267}TiO_3$ ceramic synthesized by a polymeric precursor method exhibited reasonable microwave dielectric properties, such as $\varepsilon_r = 116.2$, $Q \times f = 15{,}730$ GHz, and $\tau_f = +231$ ppm/°C.[13] Conventionally, the solid-state sintering route is applied

for ceramics processing, but a common problem associated with this method is the requirement for high calcination and sintering temperatures, causing irregular grain growth during sintering. The main advantage of fabricating ceramics by chemical routes is the formation of highly stoichiometric, pure, and homogeneous nanosized ceramic powder, ideal to achieve dense ceramics at relatively lower temperatures. The preparation and characterization of nanostructured materials have attracted increased research attention in recent years, not only for academic research but also for industrial applications, due to their unusual properties compared with materials synthesized by conventional methods.[14,15] The polymeric precursor route is simple and can be employed to produce nanosized multicomponent ceramics.[3,16,17] This method consists of formation of a polymeric complex starting from a polyhydroxy alcohol and an alpha-hydroxycarboxylic acid, with metallic cations homogeneously distributed throughout the matrix. The advantage of the polymeric precursor method is reduced segregation of different metal ions in the metal-chelate complexes. Immobilization of metal-chelate complexes in such a rigid organic polymer net can reduce segregation of individual metals during pyrolysis at high temperatures.

In the present study, the effect of $(Ca_{0.8}Sr_{0.2})_{0.6}La_{0.267}TiO_3$ on the phase constitution, microstructure, and microwave dielectric properties of $Mg_{0.95}Zn_{0.05}TiO_3$ fabricated by the polymeric precursor route was investigated.

EXPERIMENTAL PROCEDURES

Synthesis

High-purity (≥99%) magnesium nitrate $[Mg(NO_3)_2{\cdot}6H_2O]$, zinc nitrate $[Zn(NO_3)_2{\cdot}6H_2O]$, calcium nitrate $[Ca(NO_3)_2{\cdot}4H_2O]$, strontium nitrate $[Sr(NO_3)_2]$, lanthanum nitrate $[La(NO_3)_3{\cdot}6H_2O]$ (≥99%, Scharlau), ethylene glycol ($C_2H_6O_2$), and citric acid ($C_6H_8O_7{\cdot}H_2O$) were acquired from Scharlau (Barcelona, Spain), and ≥97% pure titanium isopropoxide $[Ti(C_3H_7O)_4]$ was acquired from Sigma Aldrich (Dorset, UK). Titanium citrate solution was prepared by first dissolving stoichiometric amount of $Ti(C_3H_7O)_4$ in $C_2H_6O_2$ followed by slow addition of $C_6H_8O_7{\cdot}H_2O$ in a beaker with stirring for 30 min. Citrate solution of the other metals was obtained by dissolving metal nitrates in deionized water followed by addition of citric acid. Clear solution was obtained by mixing both citrate solutions slowly while stirring at 60°C. To promote polymerization, the clear solution was kept overnight in an oven at 120°C. The solution became viscous with loss of excess solvent, and finally brown resin was obtained. To remove excess organic residue, the resin was heated at 250°C for 3 h. The resulting precursor was calcined at different temperatures (500°C, 600°C, 700°C, and 800°C) to obtain $(1-x)M_{0.95}Zn_{0.05}T$-$x(Ca_{0.8}Sr_{0.2})_{0.6}La_{0.267}TiO_3$ composite ceramic powders, hereinafter referred to as $(1-x)$MZT-xCSLT, where x is the molar fraction of CSLT. The calcined powders were ball-milled for 8 h prior to pressing into 11-mm-diameter ~5-mm-high pellets at 2000 kg/cm^2. The pellets were sintered at 1200°C at heating/cooling rate of 3°C/min.

Characterization

A Netzsch STA 409PC/PG thermal analyzer was employed for thermal analysis of the polymeric precursor at air flow rate of 50 mL/min with heating rate of 15°C/min up to 800°C. The mass and dimension method was used to calculate the densities of the sintered pellets. For structural analysis of calcined powders and sintered pellets, a Philips (PW1830 APD system) x-ray diffractometer (XRD) was used with step size of 0.05° at 5 s/step in the range of 2θ = 10° to 80°. Samples for XRD measurements were prepared by grinding sintered pellets with SiC papers (400 grade). The microstructure of calcined powders and sintered ceramics was examined using a field-emission scanning electron microscope (FE-SEM; Philips XL30). SEM samples were prepared by grinding pellets with various grades (400 to 1200) of SiC papers, and polished with diamond paste (6 μm) and an oxide polishing suspension, then etched at 1100°C for 1 h. A Renishaw microscope system (New Mills, Wotton-Under-Eagle, UK) with a 514-nm excitation laser diode, was employed to record the Raman spectra from sintered pellets at room temperature. The resonance cavity method employing an Agilent R3767CH vector network analyzer in the temperature range of 20°C to 75°C was used to measure the microwave dielectric properties of the sintered pellets.[18]

RESULTS AND DISCUSSION

Thermogravimetry

Thermogravimetry/differential scanning calorimetry (TG/DSC) curves of $(1-x)$MZT-xCSLT polymeric precursors are shown in Fig. 1. The first weight loss (~8%) was observed from room temperature to ~250°C, accompanied by an associated small endotherm on the DSC curve at 108°C. This weight loss may be attributed to removal of adsorbed water from atmosphere, decomposition of NO_3^- absorbed on the surface of the precursor, and burning of residual organics. A drastic weight loss (~66%) was observed in the temperature range of 250°C to 550°C, which may attributed to decomposition of citrate complex and nucleation of metal ions into metal oxides.[19] The DSC profile for the second weight loss appeared split into three peaks (400.4°C, 471.7°C, and 513.8°C), corresponding to combustion of citrate complex and phase formation. Thermal decomposition of citrate complex occurs as follows[20]:

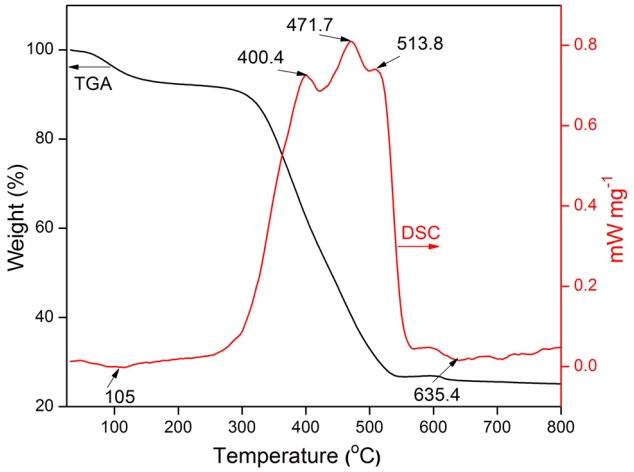

Fig. 1. TG/DSC curves for 0.8MZT-0.2CSLT polymeric precursor.

$$(Mg/Zn/Ca/Sr/La)Ti(C_6H_5O_7)_2 \rightarrow (Mg/Zn/Ca/Sr/La)TiO(C_2O_4)_2 \rightarrow (Mg/Zn/Ca/Sr/La)Ti(OH)_2C_2O_4 \quad (1)$$

The small weight loss (~1.2%) observed at temperatures up to 700°C could be assigned to solid-state reaction of residual metal carbonates and TiO_2 associated with a very small endothermic peak on DSC at 635°C.

Phase and Microstructure

XRD patterns of the $(1 - x)$MZT-xCSLT samples calcined in air atmosphere at different temperatures of 500°C, 600°C, 700°C, and 800°C are shown in Fig. 2. No XRD peaks indicative of crystallization could be seen in the XRD pattern of the sample calcined at 500°C. The emergence of all the peaks matching the relevant PDF files for the $(1 - x)$MZT-xCSLT sample calcined at 600°C indicated crystallization of the final phases, as identified by the TGA and DSC profiles. The XRD pattern of the sample calcined at 600°C revealed formation of MZT as major phase along with minor CSLT phase and impurity $MgTi_2O_5$ (MTO5) phase. When the calcination temperature was increased to 800°C, the observed increase in peak intensity for MZT and CSLT indicates an increase in the crystallinity of these phases, while the decrease in the peak intensity for MTO5 indicates a decrease in the amount of this phase. Figure 3 shows the XRD patterns of $(1 - x)$MZT-xCSLT ($x = 0$ to 0.25) ceramics sintered at 1200°C. As expected, all the XRD peaks and relevant intensities recorded for the $x = 0$ sample matched PDF# 00-006-0494 for MZT with rhombohedral (*R3*) symmetry as major phase. With an increase in x to 0.1, peaks due to CSLT with orthorhombic (*Pbnm*) symmetry (PDF # 00-022-0153) emerged and persisted throughout the employed composition range. A single low-intensity

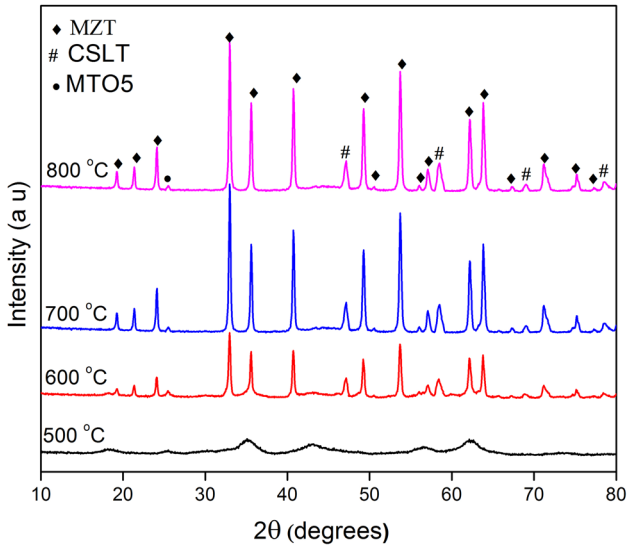

Fig. 2. XRD patterns of $(1 - x)$MZT-xCSLT powders calcined at different temperatures.

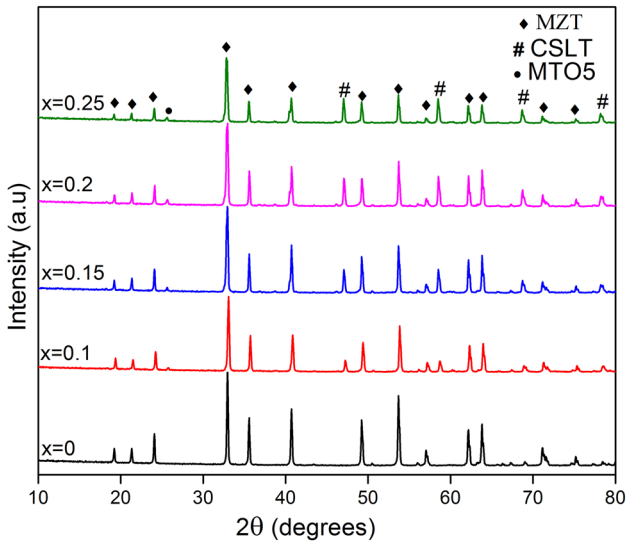

Fig. 3. XRD patterns of $(1 - x)$MZT-xCSLT ceramics sintered at 1200°C.

peak matching PDF# 00-035-0792 for the impurity phase MTO5 was observed in the XRD patterns for all samples except for $x = 0$.

Figure 4 shows the Rietveld refinement results for the $x = 0$ and 0.2 compositions. Refinement of these XRD data was carried out using MAUD software.[21] These refinements produced good agreement factors: R_{wp} = 11.08 to 8.69, R_p = 8.28 to 6.40, R_{exp} = 7.19 to 6.63, and goodness of fit of 1.49 to 1.23. The refined crystallographic data for $(1 - x)$MZT-xCSLT ($x = 0$, 0.1, 0.15, 0.2, 0.25) ceramics are listed in Table I. As is evident from Table I, there was no significant change in the lattice parameters with increasing CSLT content,

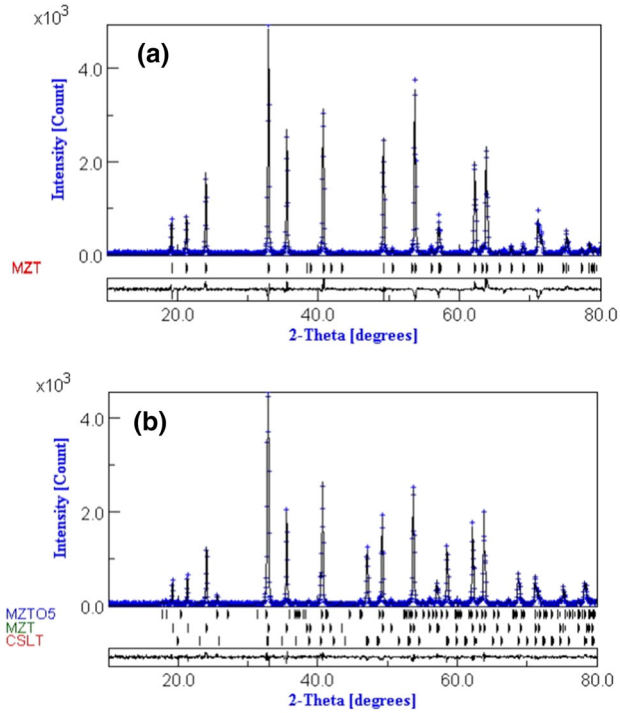

Fig. 4. Rietveld refinement of ceramics sintered at 1200°C: (a) MZT and (b) 0.8MZT-0.2CSLT.

demonstrating the formation of composite ceramics without any diffusion of CSLT into MZT. An appropriate increase in the XRD peak intensity of CSLT phase was observed, consistent with the increase in the amount of CSLT, from $x = 0.1$ to 0.25. Furthermore, the slight shift of diffraction peak positions of MZT and CSLT towards lower angles than for $MgTiO_3$[22] and $CaTiO_3$,[23] respectively, might be due to the larger ionic radius of the constituent Zn^{+2} compared with Mg^{2+} for the same coordination number (6). Similarly, the ionic radii of Sr^{+2} and La^{+3} are larger than that of Ca^{+2}.[24]

Figure 5a and b shows FE-SEM images of $(1 - x)$MZT-xCSLT ($x = 0$ and 0.2) powders calcined at 700°C. Close inspection of these images demonstrates agglomeration of relatively smaller (<100 nm) particles. Figure 5c and d shows FE-SEM images of sintered $(1 - x)$MZT-xCSLT ceramics. The microstructure of the single-phase MZT ceramic sample (i.e., $x = 0$ sintered composition) comprised densely packed grains of size ranging from 3 μm to 5 μm with no variation in contrast. On the other hand, the microstructure of the sintered composition with added CSLT comprised relatively smaller grains with further smaller grains at triple junctions, demonstrating the multiphasic nature of the sample.

Raman Spectroscopy

Raman spectra of the sintered $(1 - x)$MZT-xCSLT samples are shown in Fig. 6. The ilmenite structure of $MgTiO_3$ is known to exhibit $5A_g + 5E_g$ Raman-active vibrational modes.[25] The vibrations of Mg/Zn and Ti (A_g modes) along z-axis appeared at 223.97 cm^{-1} and 304.84 cm^{-1}. The other A_g modes associated with vibrations of O atoms were observed at 396.36 cm^{-1}, 496.31 cm^{-1}, and 714.54 cm^{-1}. The Raman mode observed at 279.3 cm^{-1} may be due to the E_g mode, an antisymmetric vibration of oxygen octahedron. The Raman modes observed at 325.06 cm^{-1} and 350.60 cm^{-1} may be due to twisting vibrations of oxygen octahedron with Mg/Zn and Ti atoms, while the mode observed at 483.62 cm^{-1} may be associated with antisymmetric vibration of Mg/Zn and Ti atoms with O octahedra, and the E_g mode at 640.05 cm^{-1} may arise from antisymmetric vibration of Ti–O stretching region.

There are 24 Raman-active modes for orthorhombic ($Pbnm$) symmetry, i.e., $7A_g + 5B_{1g} + 7B_{2g} + 5B_{3g}$.[26,27] Three weak A_g Raman modes at 161.09 cm^{-1}, 205.9 cm^{-1}, and 256.06 cm^{-1} related to bending vibration of O–Ti–O can be seen for the CSLT phase. It is possible that the other bands predicted for CSLT may be overlapped by other intense bands, or many modes have very low polarizability so as to prevent their being seen in the spectrum, as reported for $CaTiO_3$.[28,29]

Density and Microwave Dielectric Properties

The mixing model reported in Ref. 30 was used to calculate the theoretical density of the composite ceramic system comprising two phases, using Eq. 2:

$$\frac{1}{\rho} = \frac{(1-x)}{\rho_1} + \frac{x}{\rho_2}, \tag{2}$$

where x is the molar fraction of CSLT, and ρ_1 and ρ_2 are the theoretical densities of MZT and CSLT phase, respectively. The values of the theoretical density for both phases were calculated from XRD data. The dielectric constant and quality factor are closely related to the bulk density, and both are known to increase with an increase in density. The apparent densities, dielectric constants, and quality factors of the 0.8MZT-0.2CSLT ceramics sintered at different temperatures are shown in Fig. 7. The 0.8MZT-0.2CSLT composition sintered at 1200°C showed the highest relative density, i.e., 93.1% of theoretical density, and exhibited the optimum microwave dielectric properties: $\varepsilon_r = 25.17$ and $Q \times f = 58{,}754$ GHz. Figure 8a shows that the dielectric constant increased from 16.18 to 27.26 with increase in x from 0 to 0.25. The dielectric constant of ceramic composites can be predicted using different mixing models, given mathematically by Eqs. 3–5:

Parallel mixing model[31]:

$$\varepsilon_r = (1-x)\varepsilon_{r_1} + y\varepsilon_{r_2}; \tag{3}$$

Series mixing model[32]:

Table I. Refinement data for (1 − *x*)MZT-*x*CSLT ceramics sintered at 1200°C

	$Mg_{0.95}Zn_{0.05}TiO_3$					$(Ca_{0.8}Sr_{0.2})_{0.6}La_{0.267}TiO_3$			
Sample	***x* = 0**	***x* = 0.1**	***x* = 0.15**	***x* = 0.2**	***x* = 0.25**	***x* = 0.1**	***x* = 0.15**	***x* = 0.2**	***x* = 0.25**
a (Å)	5.0554	5.0564	5.0545	5.0550	5.0540	5.4681	5.4682	5.4681	5.4700
b (Å)	5.0554	5.0564	5.0545	5.0550	5.0540	5.4607	5.4675	5.4702	5.4677
c (Å)	13.9070	13.9109	13.9073	13.9076	13.9056	7.7248	7.7247	7.7254	7.7253
Structure			Hexagonal				Orthorhombic		
Space group			*R-3:H*				*Pbnm:cab*		
Crystallite size (nm)	483	468	454	444	441	–	285	311	335
Rms strain	0.00043	0.00052	0.00044	0.00040	0.00045	–	0.00042	0.00040	0.00045
Density (g/cc)	3.9566	3.9540	3.9579	3.9571	3.9592	4.6718	4.6660	4.6633	4.6640
x (Mg,Zn)/(Ca,Sr,La)	0	0	0	0	0	0.0010	−0.0054	0.00047	−0.0052
y (Mg,Zn)/(Ca,Sr,La)	0	0	0	0	0	0.0116	0.0105	0.0134	0.0114
z (Mg,Zn)/(Ca,Sr,La)	0.3586	0.3579	0.3565	0.3561	0.3574	0.25	0.25	0.25	0.25
x Ti	0	0	0	0	0	0	0	0	0
y Ti	0	0	0	0		0.5	0.5	0.5	0.5
z Ti	0.1462	0.1453	0.1443	0.1446	0.1452	0	0	0	0
x O1	0.3218	0.3214	0.3201	0.3238	0.3219	0.0152	0.0388	0.0339	0.0463
y O1	0.0288	0.0294	0.0259	0.0263	0.0295	0.5049	0.4982	0.5106	0.5020
z O1	0.2454	0.2445	0.2457	0.2448	0.0245	0.25	0.25	0.25	0.25
x O2	–	–	–	–	–	0.7917	0.7636	0.7334	0.7339
y O2	–	–	–	–	–	0.2768	0.2146	0.2720	0.2844
z O2	–	–	–	–	–	0.0360	0.0424	0.0382	0.0282

Sample	***x* = 0**	***x* = 0.1**	***x* = 0.15**	***x* = 2**	***x* = 0.25**
R_{wp} (%)	11.0833	10.5570	8.6930	8.6709	8.9167
R_p (%)	8.2861	8.1149	6.4078	6.4814	6.4925
R_{exp} (%)	6.9359	7.0833	6.6903	6.7084	7.1983
GoF	1.5979	1.4904	1.2993	1.2925	1.2387

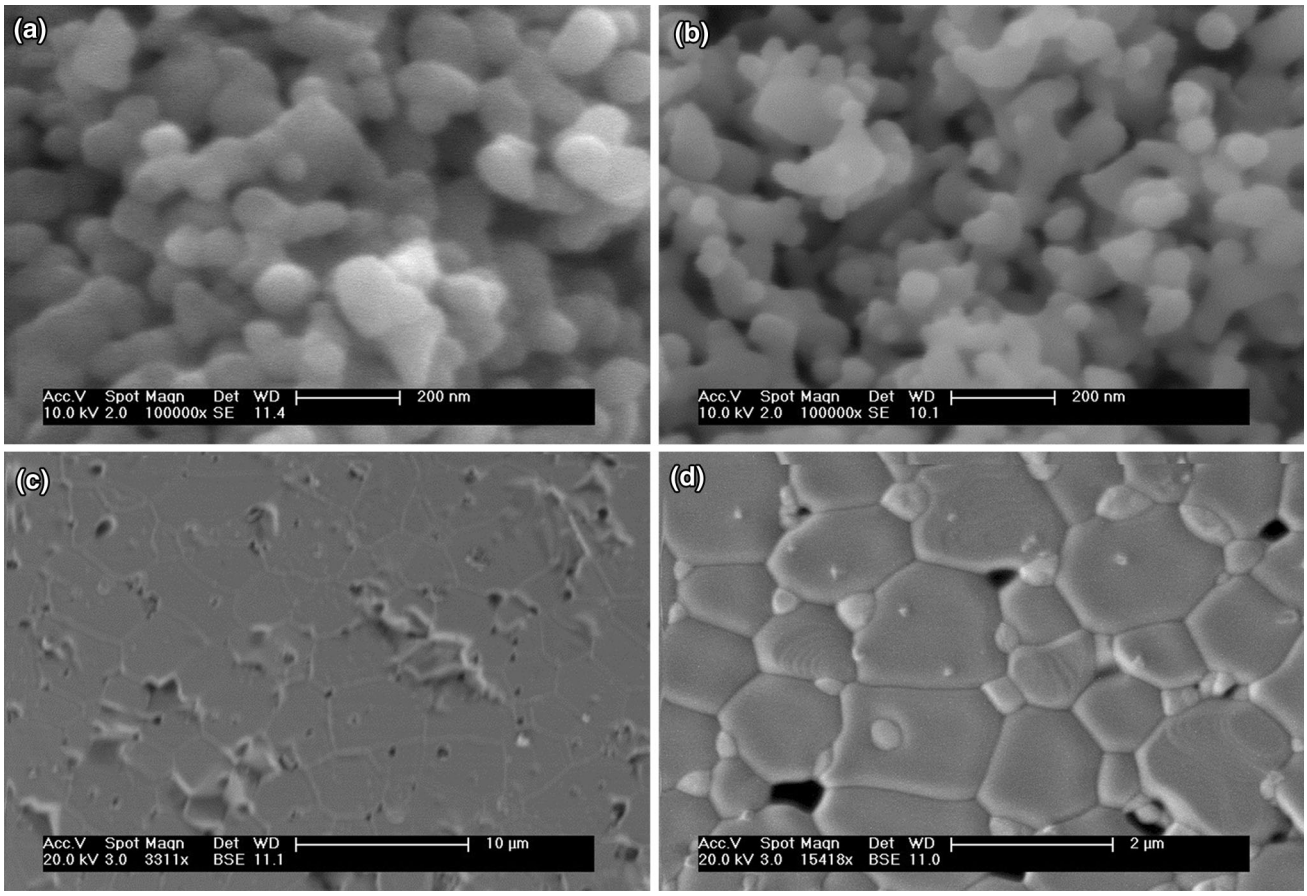

Fig. 5. FE-SEM images of powder samples calcined at 700°C: (a) MZT and (b) 0.8MZT-0.2CSLT ceramics, and sintered at 1200°C: (c) MZT and (d) 0.8MZT-0.2CSLT.

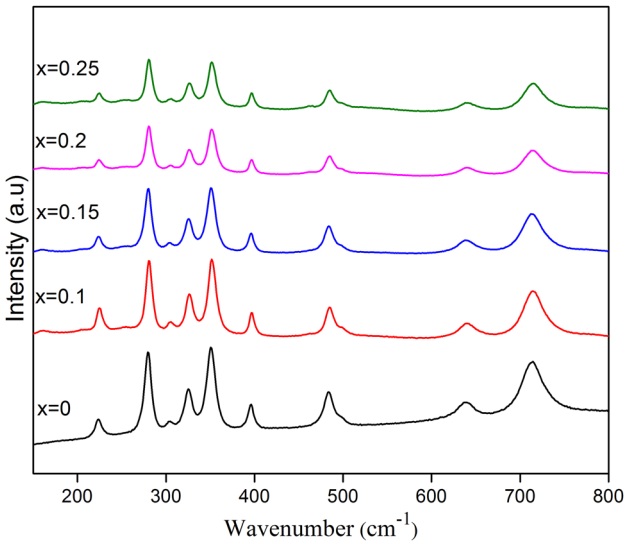

Fig. 6. Room-temperature Raman spectra of (1 − *x*)MZT-*x*CSLT ceramics.

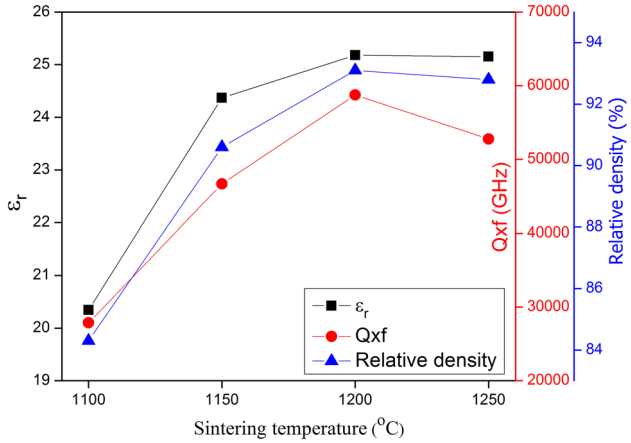

Fig. 7. Density and microwave dielectric properties of 0.8MZT-0.2CSLT ceramics with different sintering temperatures.

$$\frac{1}{\varepsilon_r} = \frac{(1-x)}{\varepsilon_{r_1}} + \frac{x}{\varepsilon_{r_2}}; \qquad (4)$$

Lichtenecker model[33]:

$$\ln \varepsilon_r = (1-y)\ln \varepsilon_{r_1} + y \ln \varepsilon_{r_2}, \qquad (5)$$

where x is the molar fraction of CSLT phase, and ε_{r1} and ε_{r2} are the dielectric constants of MZT and CSLT phase, respectively. Figure 8b shows a comparison of the calculated and experimental values of

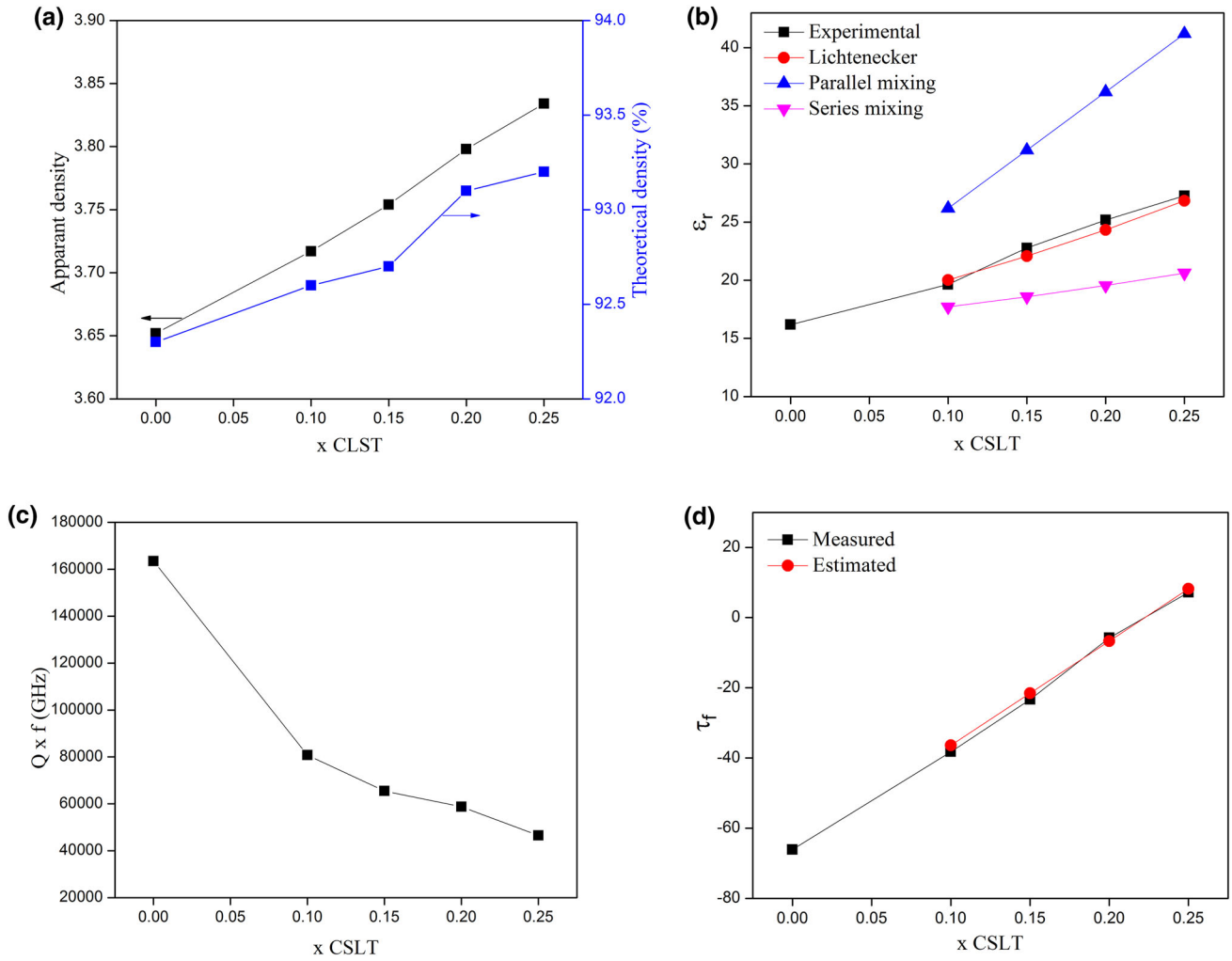

Fig. 8. (a) Density, (b) dielectric constant, (c) quality factor, and (d) temperature coefficient of resonant frequency for (1 − *x*)MZT-*x*CSLT ceramics sintered at 1200°C.

Table II. Microwave dielectric properties of (1 − *x*)MZT-*x*CSLT composite ceramics sintered at 1200°C

	Density (g/cc)					
***x* Value**	**Theoretical**	**Experimental**	**Relative %**	ε_r	$Q \times f$ **(GHz)**	τ_f **(ppm/°C)**
0	3.956	3.652	92.3	16.18	163,480	−66.1
0.1	4.015	3.717	92.6	19.63	80,765	−38.2
0.15	4.050	3.754	92.7	22.77	65,456	−23.3
0.2	4.080	3.798	93.1	25.17	58,754	−5.8
0.25	4.114	3.834	93.2	27.26	46,465	7.2

ε_r for the (1 − *x*)MZT-*x*CSLT composite ceramics for different *x* values. In the present case, it can be seen from Fig. 8a that the results obtained through the Lichtenecker theoretical model were comparatively closer to the experimental values than the other two models (Eqs. 4 and 5). In microwave dielectrics having two components, the Q is predicted by Eq. 6[34]:

$$\frac{1}{Q} = \frac{1-x}{Q_1} + \frac{x}{Q_2}, \tag{6}$$

where Q_1 and Q_2 are the quality factors of component phase 1 and 2, respectively. In the present study, the measured Q values were lower than the predicted ones. The deviation of the measured values from the predicted values may be due to

the relatively lower density, porosity, and dissimilar microstructures of the constituent phases. Figure 8c shows the quality factor values of the $(1-x)$MZT-xCSLT ceramics as a function of x. The $Q \times f$ values of the current samples decreased from 163,480 GHz to 46,465 GHz with increase in the CSLT content from $x = 0.00$ to 0.25, due to the much lower $Q \times f$ value of the CSLT phase. The dielectric loss at microwave frequencies is governed by the density, porosity, second phases, grain boundaries, and inclusions in real homogeneous ceramics.[35,36] Moreover, the higher-dielectric-constant CSLT phase exhibits higher polarizability, resulting in higher intrinsic losses, which may be a possible reason for the observed substantial decrease in $Q \times f$.

Figure 8d shows the temperature coefficient of resonant frequency (τ_f) of the sintered $(1-x)$MZT-xCSLT ceramics. There are several factors which affect τ_f, such as the composition of the ceramics, the type and amount of additives, and second phase(s). The τ_f of the composites was predicted using Eq. 7[37]:

$$\tau_f = (1-x)\tau_{f1} + x\tau_{f2}, \quad (7)$$

where x is the molar fraction of CSLT phase, and τ_{f1} and τ_{f2} are the temperature coefficients of resonant frequency of the MZT and CSLT phase, respectively. The τ_f value was observed to change from −60 ppm/°C to 7.2 ppm/°C as the molar ratio of CSLT was increased from 0 to 0.25. Figure 8d also shows that the measured values of τ_f deviated slightly from the values predicted using Eq. 7. A near-zero τ_f value (i.e., −5.8 ppm/°C) was achieved for the 0.8MZT-0.2CSLT ceramic sintered at 1200°C (Table II). Although the dielectric constant values of these $(1-x)$MZT-xCSLT ceramics are comparable to those reported for $(1-y)Mg_{0.95}Co_{0.05}TiO_3$-$y(Ca_{0.8}Sr_{0.2})_{0.6}La_{0.267}TiO_3$, i.e., $(1-y)$MCoT-yCSLT,[20] the $Q \times f$ values (163,480 GHz to 46,465 GHz for $x = 0$ to 0.25) of the $(1-x)$MZT-xCSLT ceramics achieved in the present study are higher than those (138,766 GHz to 39,180 GHz at $y = 0$ to 0.25) reported for $(1-y)$MCoT-yCSLT.[20] This observed improvement may be due to the fact that the ionic polarizability of Zn (2.04 Å) is higher than that of Co (1.65 Å), resulting in stronger atomic vibrations causing a decrease in the dielectric loss.[38]

CONCLUSIONS

$(1-x)$MZT-xCSLT powders with submicron particle size were successfully synthesized by a chemical synthesis route. XRD refinement revealed that, in the sintered composites, CSLT phase (with *Pbnm* symmetry) coexisted with MZT phase (with *R3* symmetry) along with a small proportion of MTO5 impurity phase. As expected, the dielectric constant and τ_f values increased while the $Q \times f$ value decreased with increase in the amount of CSLT. However, the $Q \times f$ value decreased with increasing CSLT amount. The 0.8MZT-0.2CSLT composition sintered at 1200°C exhibited $\varepsilon_r = 25.17$, $Q \times f = 58{,}754$ GHz, and $\tau_f = -5.8$ ppm/°C.

ACKNOWLEDGEMENTS

One of the authors acknowledges the laboratory support extended by Prof. Robert Freer, School of Materials, University of Manchester, Manchester M13 9PL, UK, for partial characterization of the materials. We acknowledge financial support extended by the Directorate of S&T, KP via ADP No. 130314 and Pilot Research Studies for the enhancement of research facilities in Materials Research Laboratory, and Mineral Upgradation Pilot Plant, University of Peshawar.

REFERENCES

1. F. Liu, X.-Y. Liu, C.-L. Yuan, J.-J. Qu, G.-H. Chen, C.-R. Zhou, and F. Liu, *J. Eur. Ceram. Soc.* 35, 2091 (2015).
2. X. Guo, B. Tang, J. Liu, H. Chen, and S. Zhang, *J. Alloys Compd.* 646, 512 (2015).
3. A. Ullah, Y. Iqbal, T. Mahmood, A. Mahmood, A. Naeem, and M. Hamayun, *Ceram. Int.* 41, 15089 (2015).
4. A. Naeem, A. Mahmood, Y. Iqbal, A. Ullah, T. Mahmood, and M. Humayun, *J. Alloys Compd.* 645, 290 (2015).
5. J. Qu, F. Liu, C. Yuan, X. Liu, and G. Chen, *Mater. Sci. Eng. B* 191, 15 (2015).
6. H. Li, B. Tang, Y. Li, Z. Qing, and S. Zhang, *Mater. Lett.* 145, 30 (2015).
7. K. Wakino, *Ferroelectrics* 91, 69 (1989).
8. C.-L. Huang, Y.-B. Chen, and C.-F. Tasi, *J. Alloys Compd.* 460, 675 (2008).
9. L. Li, J. Ye, S. Zhang, Z. Gao, and S. Li, *J. Alloys Compd.* 648, 184 (2015).
10. R. Kell, A. Greenham, and G. Olds, *J. Am. Ceram. Soc.* 56, 352 (1973).
11. I.-S. Kim, W.-H. Jung, Y. Inaguma, T. Nakamura, and M. Itoh, *Mater. Res. Bull.* 30, 307 (1995).
12. P. Wise, I. Reaney, W. Lee, T. Price, D. Iddles, and D. Cannell, *J. Eur. Ceram. Soc.* 21, 1723 (2001).
13. A. Naeem, A. Ullah, Y. Iqbal, T. Mahmood, and A. Mahmood, *J. Alloys Compd.* 672, 298 (2016).
14. W.K. Leutwyler, S.L. Bürgi, and H. Burgl, *Science* 271, 933 (1996).
15. A.L. Rogach, D.V. Talapin, E.V. Shevchenko, A. Kornowski, M. Haase, and H. Weller, *Adv. Funct. Mater.* 12, 653 (2002).
16. H. Wu, Z. Feng, Q. Mei, J. Guo, F. Hou, P. Li, and X. Jiang, *Ceram. Int.* 41, 7645 (2015).
17. Y. Liu, Y. Pu, Z. Sun, and Q. Jin, *Mater. Res. Bull.* 70, 195 (2015).
18. T. Nishikawa, K. Wakino, H. Tamura, H. Tanaka, and Y. Ishikawa, *1987 IEEE MTT-S International Microwave Symposium Digest* (1987), p. 277.
19. C. Mao, X. Dong, and T. Zeng, *Mater. Lett.* 61, 1633 (2007).
20. A. Ullah, A. Naeem, Y. Iqbal, T. Mahmood, and A. Mahmood, *J. Mater. Sci.* 27, 3506 (2016).
21. L. Lutterotti and C. Maud, *Newsletter, (IUCr)* No. 24 (December 2000).
22. M. Zhang, L. Li, W. Xia, and Q. Liao, *J. Alloys Compd.* 537, 76 (2012).
23. H. Kay and P. Bailey, *Acta Crystallogr.* 10, 219 (1957).
24. R.D. Shannon, *Acta Crystallogr. Sect. A* 32, 751 (1976).
25. C.-H. Wang, X.-P. Jing, W. Feng, and J. Lu, *J. Appl. Phys.* 104, 034112 (2008).
26. P. McMillan and N. Ross, *Phys. Chem. Miner.* 16, 21 (1988).
27. T. Hirata, K. Ishioka, and M. Kitajima, *J. Solid State Chem.* 124, 353 (1996).
28. S. Keshri and S.S. Rajput, *Ceram. Int.* 40, 4257 (2014).
29. U. Balachandran and N. Eror, *Solid State Commun.* 44, 815 (1982).

30. H. Rocha, F.N.A. Freire, M.R.P. Santos, J.M. Sasaki, T. Cordaro, and A.S.B. Sombra, *Phys. B* 403, 2902 (2008).
31. P. Sarah and S. Suryanarayana, *Bull. Mater. Sci.* 26, 745 (2003).
32. D. Barrow, T. Petroff, R. Tandon, and M. Sayer, *J. Appl. Phys.* 81, 876 (1997).
33. Z. Hashin and S. Shtrikman, *J. Appl. Phys.* 33, 3125 (1962).
34. S.H. Yoon, G.-K. Choi, D.-W. Kim, S.-Y. Cho, and K.S. Hong, *J. Eur. Ceram. Soc.* 27, 3087 (2007).
35. D.A. Sagala and S. Nambu, *J. Am. Ceram. Soc.* 75, 2573 (1992).
36. B. Silverman, *Phys. Rev.* 125, 1921 (1962).
37. A. Paladino, *J. Am. Ceram. Soc.* 54, 168 (1971).
38. H.-J. Hagemann, *J. Phys. C* 11, 3333 (1978).